Supplementary Information

Unveiling Giant Hidden Rashba Effects in Two-Dimensional Si_2Bi_2

Seungjun Lee and Young-Kyun Kwon*

Department of Physics and Research Institute for Basic Sciences,

Kyung Hee University, Seoul, 02447, Korea

(Dated: November 10, 2020)

SUPPLEMENTARY NOTE 1

To check what the orbital polarization is for each band state, we visualized the orbital polarization by evaluating $\langle\psi_{n,\mathbf{k}}|\mathbf{L}^{\alpha}|\psi_{n,\mathbf{k}}\rangle$, the expectation value of the orbital angular momentum (OAM) operator defined by

$$L_i^{\alpha} = -i\hbar \sum_{j,k} \epsilon_{ijk} |p_j^{\alpha}\rangle\langle p_k^{\alpha}|,$$

where $i, j, k = x, y, z$; ϵ_{ijk} is the Levi-Civita symbol; and $|p_j^{\alpha}\rangle$ is the p_j orbital state at atom site α.[1] This is essentially the same procedure as done for the spin polarization, which we described in the note [24] in the Reference section in the main text.

Supplementary figure 4 shows the orbital polarization maps in the absence of SOC for the two structures shown Fig. 2 in the main text. The lowest conduction band (CB1) of 2D SiBi monolayer, which is doubly-degenerate without SOC, is contributed mostly by the Bi p_z orbitals, as shown in Fig. 2 (b) in the main text, resulting in significant OAM contribution. Thus the map of its OAM distribution (Supplementary Fig. 4 (a)) clearly exhibits the momentum-locked orbital polarization, which is exactly what we expected from the orbital Rashba Hamiltonian given in Eq. (2) in the main text. For $\mathcal{I}$-Si_2Bi_2, on the other hand, the sublayer-sublayer interaction splits four-fold degenerate conduction bands into two doubly-degenerate bands, CB1 and the second lowest conduction band (CB2), in which the Bi p_z orbital contribution is small and large, respectively, as shown in Fig. 2 (e) in the main text. Therefore, the orbital polarization is more vivid in CB2 (red arrows) than in CB1 (blue arrows), regardless of either the top or bottom Bi sublayer, but two sublayers exhibit their OAM distributions with the opposite chirality, as shown in Supplementary Fig. 4 (b) and (c), indicating that the total OAM of the whole system on each band will disappear. Therefore, $\mathcal{I}$-Si_2Bi_2 exhibits "hidden" orbital polarization or orbital-layer locking even without SOC.

With SOC on, we also computed the orbital polarizations of not only 2D SiBi monolayer, but also $\mathcal{I}$-Si_2Bi_2. Figure below (Supplementary Fig. 5) shows their calculated OAM distributions as well as their spin angular momentum (SAM) distributions for comparison, when SOC is weak (a–c) and strong (d–f). The OAM maps for weak SOC are essentially the same as those in Supplementary Fig. 4 without SOC, except that the monolayer case revealed the band-split polarizations due to weak SOC. Since the 2D SiBi does not have inversion sym-

metry, even weak SOC ($\lambda = 0.01\lambda_0$) split its spin-degenerate conduction band (CB1) into two spin polarized states, CB1 and CB2, even though their energy difference is negligibly small. Its SAM map displays that the spin polarizations on CB1 and CB2 are of the same magnitude with the opposite chirality, whereas the orbital polarizations on CB1 and CB2 are not only of the same magnitude, but also of the same chirality. Both maps clearly display the spin- and orbital-momentum locking on respective bands. For $\mathcal{I}$-Si_2Bi_2, the SAM maps projected on the top and bottom Bi atoms do not show any noticeable spin polarization as shown in Supplementary Fig. 5 (b) and (c), since the weak SOC cannot lift any one of the spin-degenerate CB1 and CB2, which are significantly separated by the sublayer-sublayer interaction and guaranteed by inversion symmetry. However, the spatially-projected OAM mpas clearly show hidden orbtial polarizations or orbtial-layer locking as mentioned above for the case without SOC.

Supplementary Figure 5 (d–f) shows the OAM and SAM maps with strong SOC. For the monolayer structure, its spin polarizations on CB1 and CB2 remain strong with a smalll difference in magnitude at each k-point, due to the Rashba splitting, and its OAM map still shows the momentum-locked polarization, which is not perfectly chiral though. For $\mathcal{I}$-Si_2Bi_2, its spatially-projected SAM maps clearly displays the hidden spin polarizations or spin-layer locking on both CB1 and CB2 induced by local broken inversion symmetry together with strong SOC. In its spatially-projected OAM maps, it was shown that the chirality of the orbital polarization (CB1+CB2) on one Bi atom sublayer is opposite to that on the other sublayer similar to those with weak SOC, however the chirality of the polarization on one sublayer is not completely opposite to that on the other on both CB1 and CB2 resulting in small, but non-zero polarization on each k-point.

SUPPLEMENTARY NOTE 2

To better describe the hidden Rashba (R-2) effect, we devised a simple model Hamiltonian, which explicitly takes into account not only Rashba splitting, but also the sublayer-sublayer (SL-SL) interaction. Our model Hamiltonian $\mathcal{H}$ can be decomposed into

$$\mathcal{H} = \mathcal{H}_0 + \mathcal{H}_{\rm R} + \mathcal{H}_{\rm I},$$

where three subscripts 0, R, and I indicate an unperturbed (free electron), Rashba spin splitting given in Eq. (1) in the main text, and SL-SL interaction, respectively. Simply, $\mathcal{H}_0$ becomes $\hbar^2k^2/2m^*$ with m^* an effective mass. For the matrix representation, we used four basis vectors $|\mathrm{T},\uparrow\rangle$, $|\mathrm{T},\downarrow\rangle$, $|\mathrm{B},\uparrow\rangle$, and $|\mathrm{B},\downarrow\rangle$ indicating states of electrons at top (T) and bottom (B) SLs with spin up ($\uparrow$) and down ($\downarrow$), respectively.

Due to the oppositely-aligned local dipole moments at the top and bottom SLs, $\mathcal{H}_R$ can be represented by

$$\langle \mathrm{T},\uparrow|\mathcal{H}_\mathrm{R}|\mathrm{T},\uparrow\rangle = -\alpha_\mathrm{R}k \qquad \langle \mathrm{T},\downarrow|\mathcal{H}_\mathrm{R}|\mathrm{T},\downarrow\rangle = \alpha_\mathrm{R}k$$
$$\langle \mathrm{B},\uparrow|\mathcal{H}_\mathrm{R}|\mathrm{B},\uparrow\rangle = \alpha_\mathrm{R}k \qquad \langle \mathrm{B},\downarrow|\mathcal{H}_\mathrm{R}|\mathrm{B},\downarrow\rangle = -\alpha_\mathrm{R}k$$

where α_R and k are Rashba strength parameter and crystal momentum. On the other hand, $\mathcal{H}_\mathrm{I}$ can be expanded, without losing generality, as

$$\mathcal{H}_\mathrm{I} = E_\mathrm{I}^0 + E_\mathrm{I}^1k^2 + E_\mathrm{I}^2k^4 + \cdots .$$

Since we consider the Hamiltonian for small k, the matrix elements of $\mathcal{H}_I$ becomes up to the 2nd order,

$$\langle \mathrm{T},\uparrow|\mathcal{H}_\mathrm{I}|\mathrm{B},\uparrow\rangle = E_\mathrm{I}^0 + E_\mathrm{I}^1k^2, \qquad \langle \mathrm{T},\downarrow|\mathcal{H}_\mathrm{I}|\mathrm{B},\downarrow\rangle = E_\mathrm{I}^0 + E_\mathrm{I}^1k^2.$$

Note that the opposite spin states on the different SLs may not give repulsive SL-SL interactions, and thus $\langle \mathrm{T},\uparrow|\mathcal{H}_\mathrm{I}|\mathrm{B}\downarrow\rangle = 0$, and so on. Thus, the total Hamiltonian ($\mathcal{H}$) becomes,

$$\mathcal{H} = \mathcal{H}_0 + \mathcal{H}_\mathrm{R} + \mathcal{H}_\mathrm{I} = \begin{pmatrix} \frac{\hbar^2k^2}{2m^*} - \alpha_\mathrm{R}k & 0 & E_\mathrm{I}^0 + E_\mathrm{I}^1k^2 & 0 \\ 0 & \frac{\hbar^2k^2}{2m^*} + \alpha_\mathrm{R}k & 0 & E_\mathrm{I}^0 + E_\mathrm{I}^1k^2 \\ E_\mathrm{I}^0 + E_\mathrm{I}^1k^2 & 0 & \frac{\hbar^2k^2}{2m^*} + \alpha_\mathrm{R}k & 0 \\ 0 & E_\mathrm{I}^0 + E_\mathrm{I}^1k^2 & 0 & \frac{\hbar^2k^2}{2m^*} - \alpha_\mathrm{R}k. \end{pmatrix}$$

To obtain its energy eigenvalues, we solved its characteristic equation $|\mathcal{H} - E\mathcal{I}| = 0$ to get

$$E_\pm = \frac{\hbar^2k^2}{2m^*} \pm \sqrt{(\alpha_\mathrm{R}k)^2 + (E_\mathrm{I}^0 + E_\mathrm{I}^1k^2)^2}, \tag{1}$$

which are two doubly-degenerate solutions satisfying the degenerate condition guaranteed by the inversion symmetry. These two equations correctly reproduce two asymptotic band behaviors, such as Rashba-like bands for $\mathcal{H}_\mathrm{I} \approx 0$ and two parabolic bands for $\mathcal{H}_\mathrm{R} \approx 0$. The parameters in Eq. (1) were determined by fitting the lowest conduction band (CB1) and

second lowest one (CB2) computed by our first-principles calculation shown in Fig. 3 (a) in the main text as follow. From bands without SOC, m^* and $E_{\rm I}^1$ were first determined to be $m^* = 0.15m_e$ and $E_{\rm I}^1 = 12.83$ eVÅ^2, respectively. With these values fixed, $\alpha_{\rm R}$ and $E_{\rm I}^0$ were then determined for nonzero SOC cases and summarized in Fig. 3 (b) in the main text.

---

* Corresponding author. E-mail: ykkwon@khu.ac.kr

[1] J. Ryoo and C. Park, NPG Asia Mater. **9**, e382 (2017).

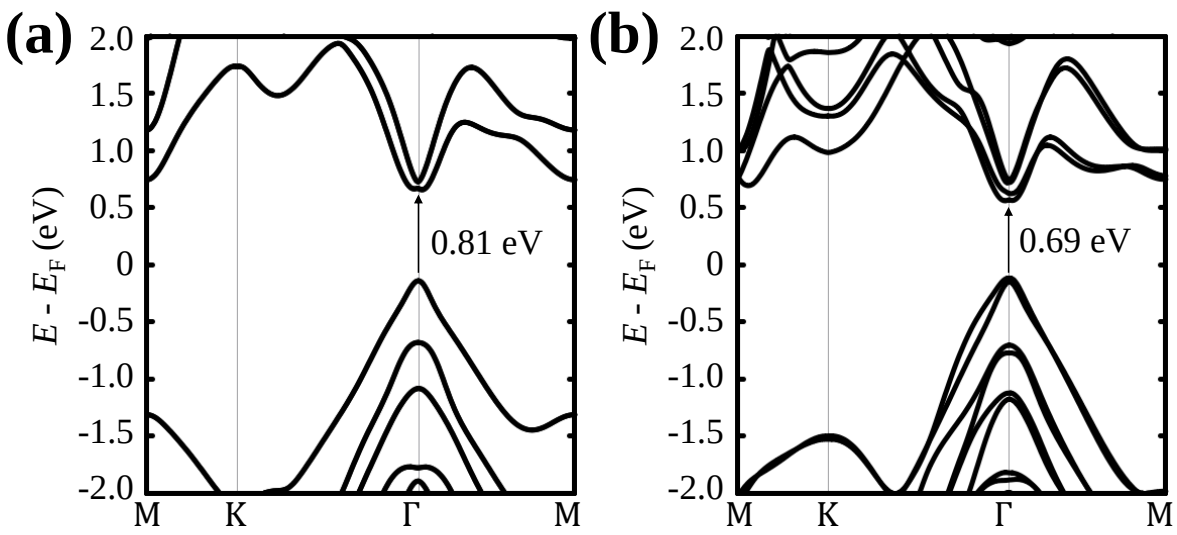

Supplementary Figure 1 Electronic band structures of (a) $\mathcal{I}$- and (b) $\mathcal{M}$-Si_2Bi_2 calculated by HSE06 functional. The calculated band gap values at the Γ point are 0.81 and 0.69 eV, respectively.

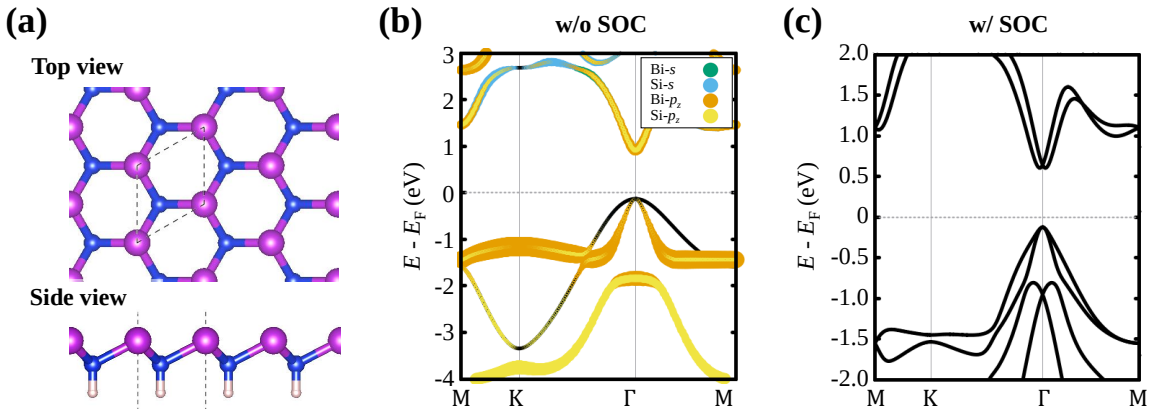

Supplementary Figure 2 (a) Top and side views of the crystal structure of 2D SiBi with same lattice constants with $\mathcal{I}$-Si_2Bi_2. The dangling bonds of Si are terminated by hydrogen atoms. The dashed lines indicate the primitive unit cell. The electronic structure of 2D SiBi is calculated by PBE functional without spin-orbit coupling (SOC) (b) and with SOC (c). Bands in (b) were resolved into different orbitals as indicated in the inset. The line thickness indicates the degree of the orbital contribution.

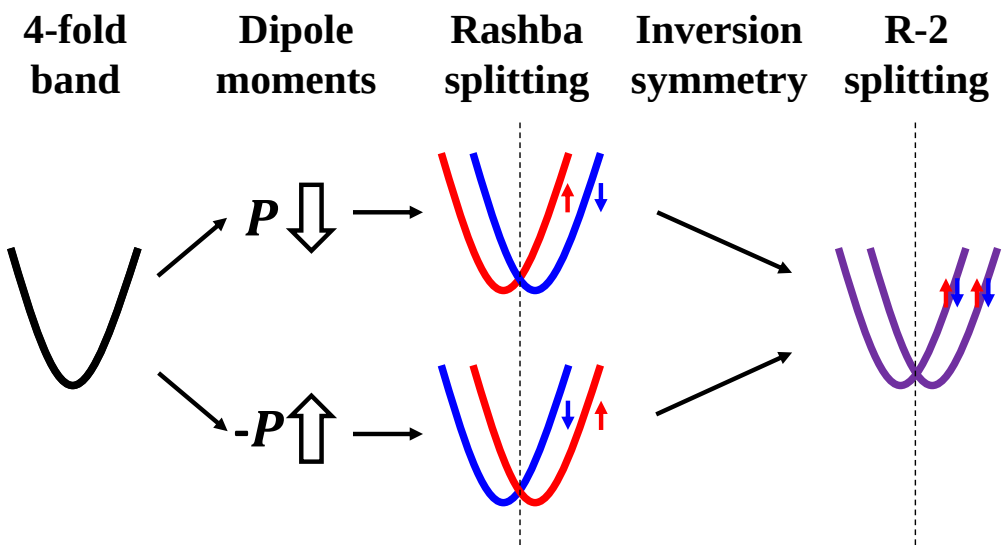

Supplementary Figure 3 Simple schematic band diagrams showing how R-2 spin splitting occurs without sublayer-sublayer (SL-SL) interaction. Without SOC, four bands from two spins and two SLs should be degenerate. Since the local symmetry breaking generates a local dipole moment on one SL, which points oppositely to that on the other one, SOC induces the local Rashba spin splitting on each SL, depicted by red and blue band lines and arrows. The split spins are oppositely aligned due to the opposite dipole field directions. The inversion symmetry guarantees the degeneracy between the inversion partners, these bands should be combined into the purple band lines representing the hidden Rashba (R-2) spin splittings leading to the spatially-separated spin-up and down states or the spin layer locking (SLL).

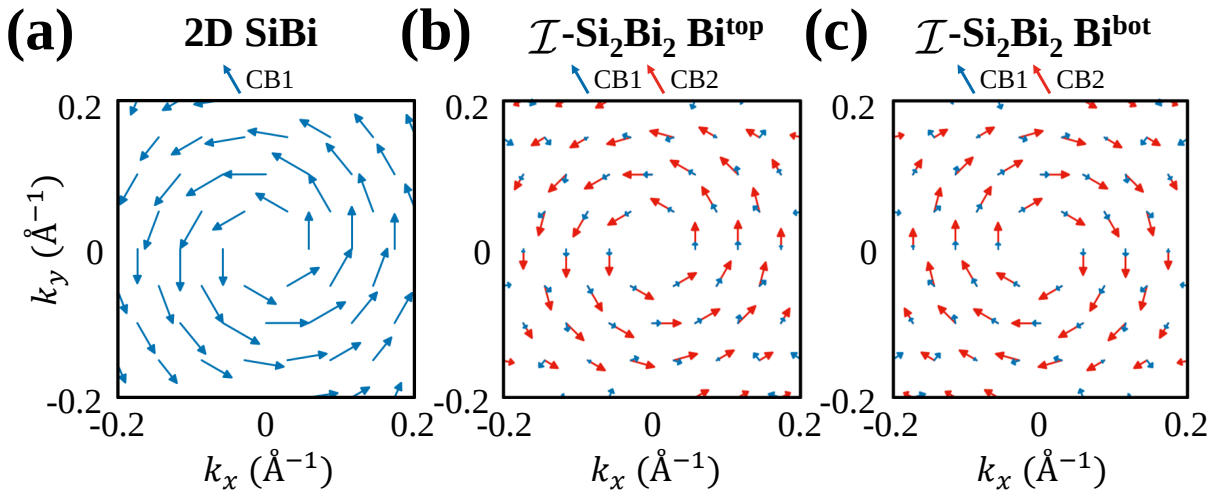

Supplementary Figure 4 The orbital polarization maps of (a) the 2D SiBi monolayer, and from (b) the top and (c) bottom Bi atoms of $\mathcal{I}$-Si_2Bi_2, near the Γ point in the absence of SOC. The blue and red arrows in each map indicate the orbital polarization evaluated on the lowest conduction band (CB1) and second lowest conduction band (CB2), respectively.

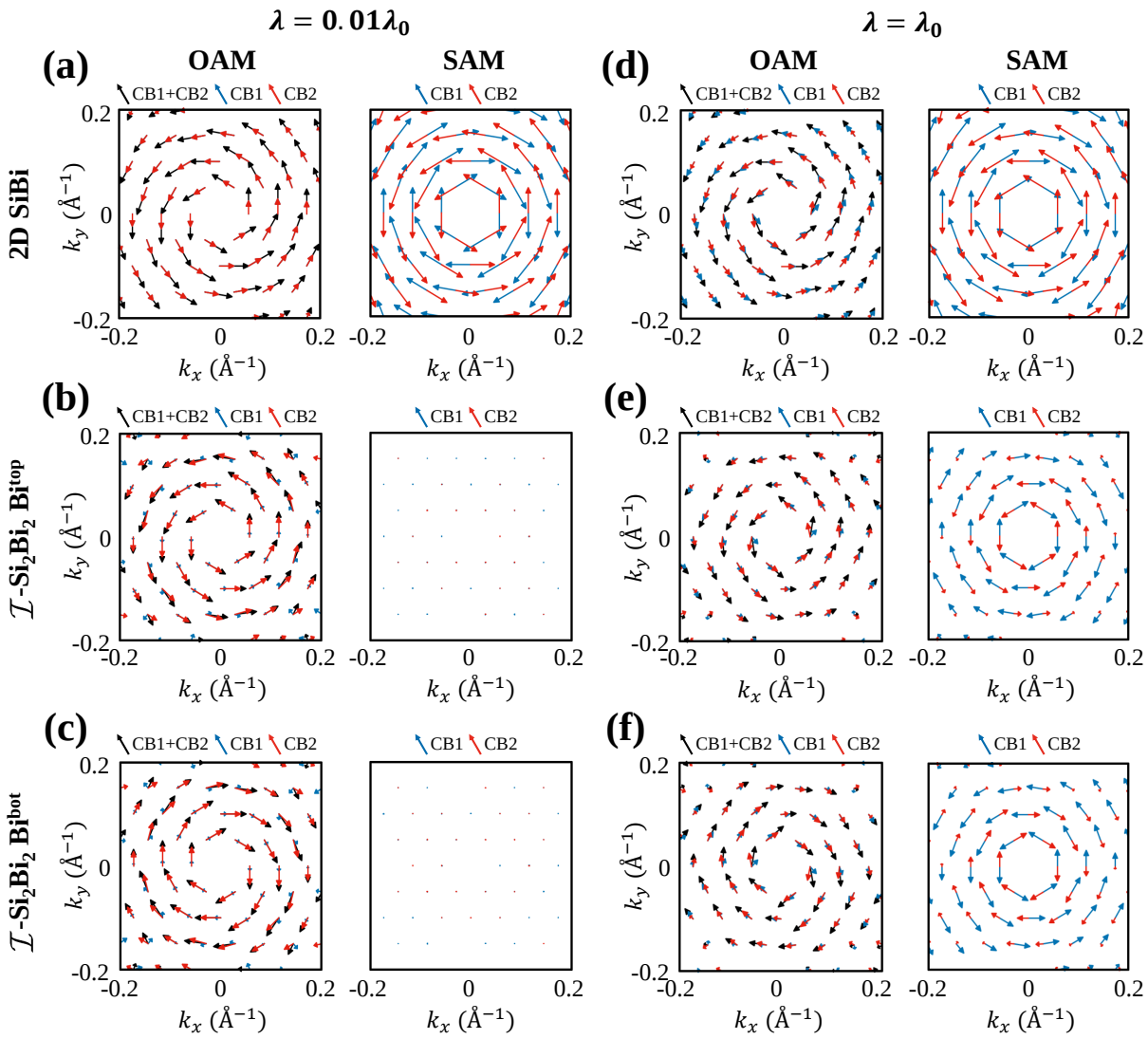

Supplementary Figure 5 The orbital angular momentum (OAM) and spin angular momentum (SAM) distributions when SOC is weak ($\lambda = 0.01\lambda_0$) (a–c) and strong ($\lambda = \lambda_0$) (d–f). The maps in the first low (a, d) display the orbital and spin polarizations of the 2D SiBi, and those in the second (b, e) and third lows (c, f) represent the polarizations projected on the top and bottom Bi atoms of $\mathcal{I}$-Si_2Bi_2, respectively. The maps in (a–c) are essentially the same as those in Fig. 4 due to weak SOC, except for small band splitting. The blue and red arrows in each map indicate the polarization evaluated in CB1 and CB2, respectively, and the black arrows represent the sum of orbital polarizations in CB1 and CB2.

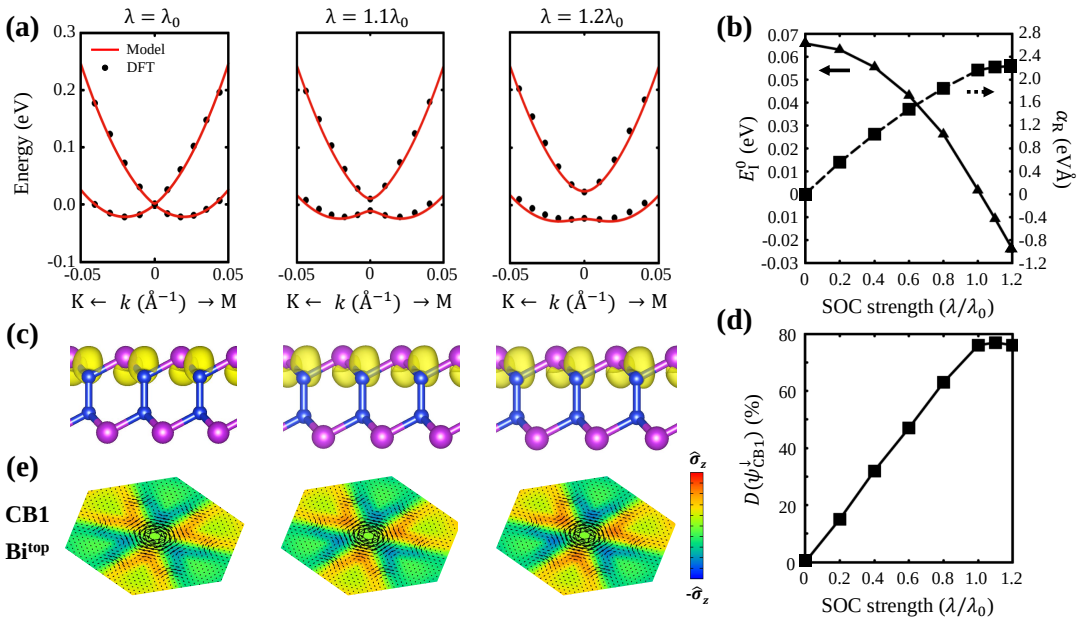

Supplementary Figure 6 Extension of Fig. 3 in the main manuscript: Evolution of the electronic structure with the SOC strength $\lambda/\lambda_0 \in (1, 1.2)$, where λ_0 is the real SOC strength: (a) two lowest conduction bands near the Γ point. The black dots show the energy eigenvalues calculated by DFT, which were fitted by the model defined in the Eq. (3) in the manuscript, plotted with red solid lines. (b) λ-dependence of the interaction energy (E_{I}^0) and the Rashba strength (α_{R}) fitted in (a). (c) $|\psi_{\mathrm{CB1}}^{\downarrow}|^2$, spin-resolved wavefunction squared, calucated at $\mathbf{k}_{\mathbf{\Gamma-M}} = (0.015, 0)(2\pi/a)$ near the Γ point. (d) Degree of wavefunction segregation D(ψ) defined in Eq. (4) in the manuscript evaluated from (c) as a function of λ. (e) Spatially-resolved spin maps on the top Bi atom layer plotted in the first Brillouin zone for the lowest conduction band. The size of black arrows and different colors indicate the in-plane and out-of-plane spin components

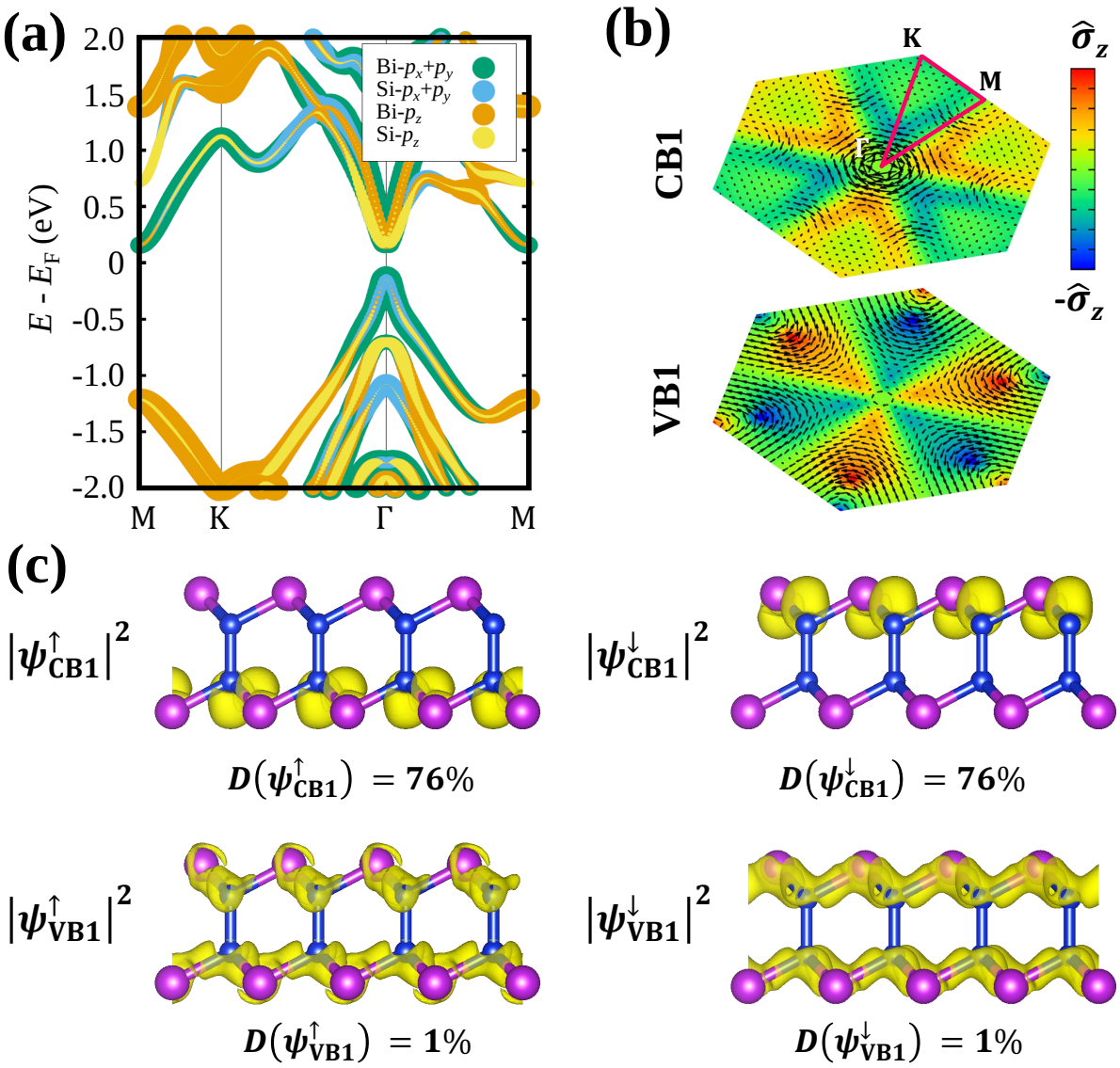

Supplementary Figure 7 (a) Orbital resolved band structure of $\mathcal{I}$-Si_2Bi_2. As indicated in the inset, each color is assigned to each projected orbital and the line thickness indicates the degree of the orbital contribution. (b) Spatially-resolved spin maps for the top Bi atom layer plotted in the first Brillouin zone for the lowest conduction band (CB1) and the highest valence band (VB1). The size of black arrows and different colors indicate the in-plane and out-of-plane spin components. (c) Real-space spinor wavefunction squared $|\psi_n^\sigma|^2$ calculated at $\mathbf{k}_{\Gamma-\mathrm{M}} = (0.015, 0)(2\pi/a)$ near the Γ point, with band index n and spin index σ. D(ψ) defined in Eq. (5) in the main text represents the degree of wavefunction segregation between the top and bottom SLs

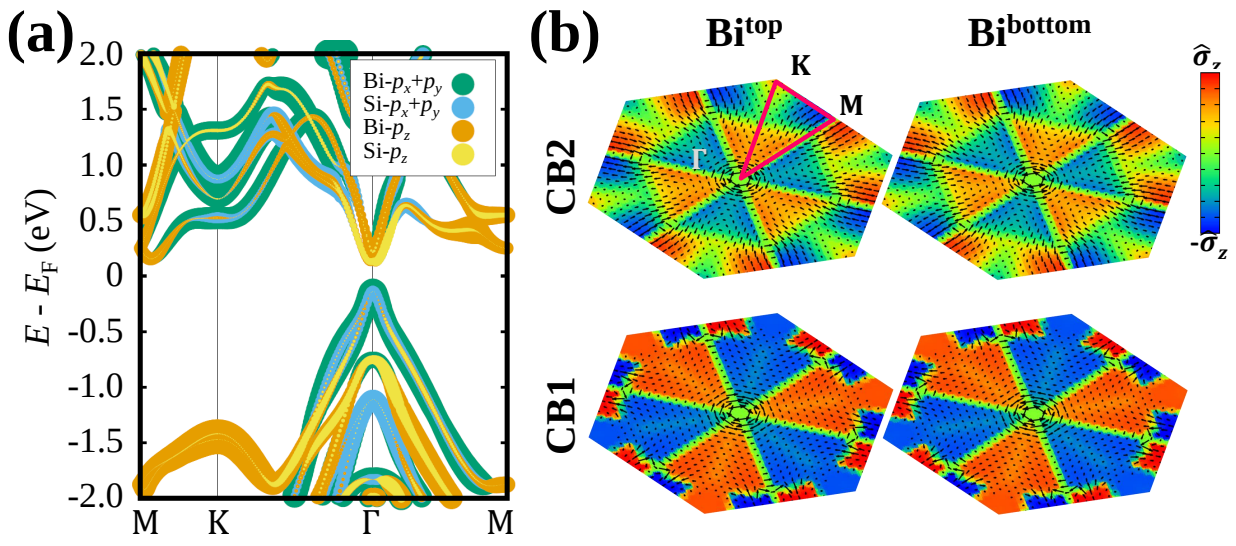

Supplementary Figure 8 The spin moment distribution for the CB1 and CB1 projected on Bi atoms in the top and bottom sublayers. The hexagonal maps represent the first Brillouin zone of $\mathcal{I}$-Si_2Bi_2, and the black arrows and color contour indicate in-plane and out-of-plane spin-polarization components, respectively. (a) Orbital resolved band structure of $\mathcal{M}$-Si_2Bi_2. As indicated in the inset, each color is assigned to each projected orbital and the line thickness indicates the degree of the orbital contribution. (b) Spatially-resolved spin maps for the top and bottom Bi atom layers plotted in the first Brillouin zone for the lowest conduction band (CB1) and the second loweset one (CB2). The size of black arrows and different colors indicate the in-plane and out-of-plane spin components.